Fabrication of Boron-Doped Diamond Nanorod Forest Electrodes and Their Application in Nonenzymatic Amperometric Glucose Biosensing

Daibing Luo,[†,‡] Liangzhuan Wu,[†] and Jinfang Zhi[†,*]

[†]Key Laboratory of Photochemical Conversion and Optoelectronic Materials, Technical Institute of Physics and Chemistry and [‡]Graduate University of Chinese Academy of Sciences, No. 2, Beiyitiao, Zhong-guan-cun, Haidian District, Beijing 100190, China

ABSTRACT A boron-doped diamond nanorod forest (BDDNF) electrode has been fabricated by hot filament chemical vapor deposition (HFCVD) method. This BDDNF electrode exhibits very attractive electrochemical performance compared to conventional planar boron-doped diamond (BDD) electrodes, notably improved sensitivity and selectivity for biomolecule detection. The BDDNF electrode, with the possibility of fabricating a sensitive biosensor for glucose without any catalyst or mediators, shows good activity toward direct detection of glucose by simply putting the bare BDDNF electrode into the glucose solution. Furthermore, the marked selectivity of the BDDNF electrode is very favorable for the determination of glucose in the presence of ascorbic acid (AA) and uric acid (UA). The robust sensitive and selective responses of this nanostructure indicate the promise of this kind of diamond electrode for real applications.

KEYWORDS: boron-doped diamond nanorod forest electrode · glucose · electrochemical detection

BDD electrodes possess excellent electrochemical properties, such as low and stable background current, wide working potential window, superb physical and chemical stability, and good biocompatibility.[1,2] Until now, planar BDD thin film electrodes have been the most studied form of diamond electrodes.[3] The planar BDD electrodes, with different surface morphologies, including microcrystalline and nanocrystalline films, have been prepared for a wide range of electrochemical applications.[4,5] However, even though the planar BDD electrodes are suitable for many electroanalytical detection, most practical applications require use of some kinds of electrodes with high surface areas to achieve high sensitivity and selectivity.[6,7]

In the past decade, nanostructured materials have been of both fundamental and technological interest because of their special characteristics, which differ markedly from their corresponding bulk states in physical and chemical performance. Nanostructured materials are considered to be much more efficient and selective than traditional bulk materials for their high surface areas and high surface energy.[8,9] For example, many carbon-based nanostructured materials have been shown to be ideal for biosensing applications since they are conductive, biocompatible, easily functionalized, and possess very large surface areas.[10,11] However, the main disadvantage of these carbon-based materials is nonstability of potential, which remains a limiting factor. Therefore, it is of interest to inquire if BDD electrodes with much smaller lateral dimensions can be fabricated, and what properties such electrodes might possess. We can cite the literature on the fabrication of nanostructured diamond films, such as diamond nanowhiskers and nanorods obtained by microfabrication methods involving RIE (reactive ion etching) or plasma etching on diamond films,[12−15] and homoepitaxially grown diamond nanorods produced by CVD technique using template methods.[16,17] However, conductive nanostructured diamond films used in electro- or biochemistry applications have seldom been reported up to now.

On the other hand, electrochemical sensors for glucose fall into two major types, that is, enzymatic and nonenzymatic metal-modified sensors. The disadvantages of these sensors are their lack of stability due to the intrinsic nature of enzymes and poisoning of metal-modified electrodes by adsorbed intermediates.[18−20] To address these problems, many attempts have been made to develop glucose sensors without using enzyme methods, and some nanostructured electrodes have been reported to develop innovative nonenzymatic glucose

*Address correspondence to zhimail@mail.ipc.ac.cn.

Received for review March 29, 2009 and accepted July 10, 2009.

Published online July 21, 2009.
10.1021/nn9003154 CCC: $40.75

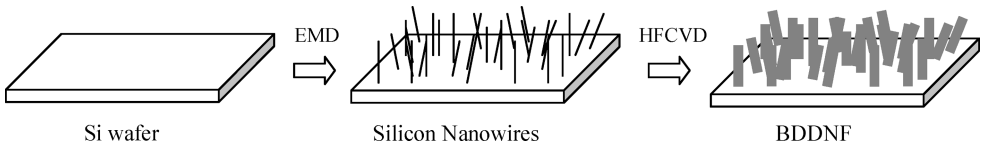

Scheme 1. Plots of fabrication of the boron-doped diamond nanorod forest (BDDNF).

sensors.[21,22] Recently, Park *et al.* reported that mesoporous Pt electrodes showed tremendous improvement in sensitivity to glucose compared to common interfering species;[23] Yuan *et al.* have prepared nanotubular Pt array electrodes, possessing high sensitivity to glucose, due to their high surface roughness factor and particular structure,[24] *etc*. Therefore, the progress which was made on nanostructured Pt-based electrodes in nonenzymatic glucose sensing gives us one of the most important clues; that is, an electrode with a high active surface area and roughness factor may be a very attractive sensor in the electro-detection of glucose.

Here, we report for the first time the fabrication and characterization of a boron-doped diamond nanorod forest electrode and the study of its electrochemical applicability in nonenzymatic amperometric detection of glucose. We combined the electroless metal deposition (EMD) method and HFCVD technique to prepare the BDDNF on silicon nanowires (SiNWs), that is, transforming a planar BDD electrode to a three-dimensional structured diamond electrode, as shown in Scheme 1. The as-fabricated BDDNF electrode was characterized using scanning electron microscopy (SEM), transmission electron microscopy (TEM), Raman spectroscopy, and cyclic voltammetry (CV) measurements. To evaluate the properties of the BDDNF electrode as a biosensor for electrochemical applications, its nonenzymatic amperometric detection of glucose was studied and compared with a planar BDD electrode. The BDDNF electrode showed excellent nonenzymatic electrochemical activity toward glucose in basic solution. Furthermore, we also demonstrated that the BDDNF electrode could selectively detect glucose in the presence of potential interfering agents such as AA and UA.

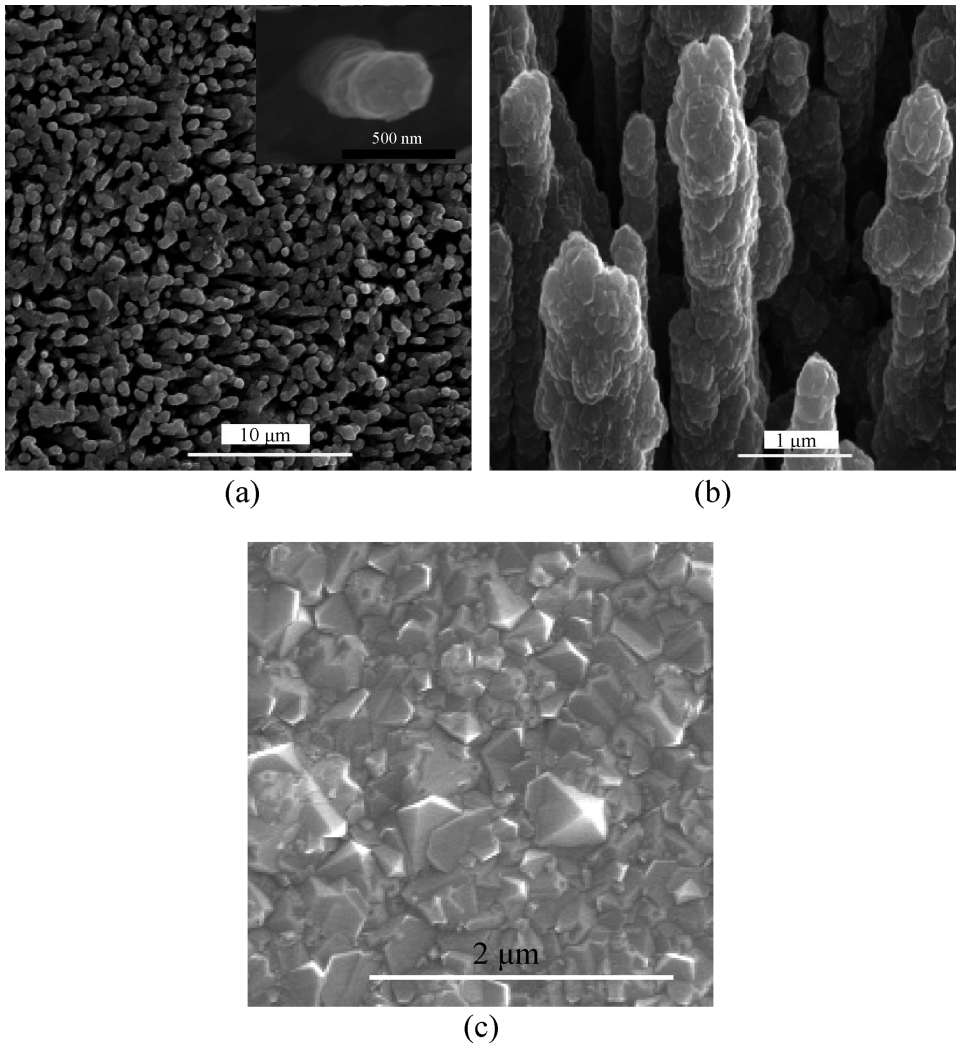

Figure 1. SEM images of (a) top and (b) side views of the BDDN; the inset graph of (a) is an amplified image of a single standing nanorod, (c) a planar BDD film deposited under the same conditions.

RESULTS AND DISCUSSION

Surface Morphology and Raman Analysis. The morphologies and microstructures of the BDDNF and BDD films were examined with SEM and TEM. As shown in Figure 1a, a large amount of boron-doped diamond nanorods standing vertically on a silicon wafer can be observed for the BDDNF, and one single nanorod from the top view is clearly observed in an inset graph of Figure 1a. The coverage of a nanocrystalline diamond film is complete and continuous along the whole length (about 5 μm) of the SiNWs. These nanorods possess rough and irregular surface and present polycrystalline morphology, as shown in Figure 1b.

Figure 1c represents a SEM image of a planar BDD film deposited under the same conditions. The BDD film with larger crystallite than the BDDNF can be observed in Figure 1c. Therefore, a difference of the

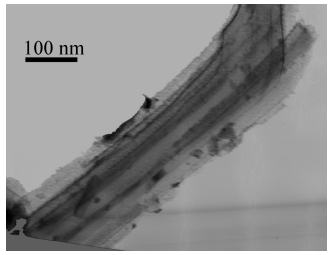

Figure 2. Typical TEM image of a BDDN.

average grain size of diamond crystallite is observed for the boron-doped diamond nanorod (BDDN) and the BDD film, related to the surface morphologies which influence the electrode surface areas. This is due to the difference of homoepitaxial growth of diamond on various silicon facets. It has been reported that diamond growth on a single-crystal substrate (Si wafer, 100) with low surface damage seems to be favorable for fabricating high crystalline quality films because it avoids crystal lattice mismatch.[25,26]

The TEM observation, carried out on an isolated nanorod scratched from the as-grown product, is shown in Figure 2, from which we can easily observe the structure of an inner silicon nanowire core, and the core region is conformally coated with polycrystalline diamond grains (sheath).

Figure 3 shows the Raman spectra of diamond films grown on the silicon nanowires for BDDN and the bulk silicon substrate for BDD. A clear and intense band at 1332 cm^{-1}, which corresponds to the one-phonon sp^3 carbon, represents the diamond characteristic peak. The full width at half-maximum of this peak is ~550 cm^{-1} for the BDDN film deposited on the silicon nanowires and ~300 cm^{-1} for the BDD film grown on the bulk silicon substrate. A larger half-maximum for the film deposited on silicon nanowires is indicative of a higher defect density because, to a first approximation, the peak width is inversely related to the phonon lifetime (*i.e.*, phonon scattering by grain boundaries and defects).[27] The feature at 1580 cm^{-1} is attributed to the graphite basal plane G band, which is well-known for disordered carbon films and arises from the in-plane

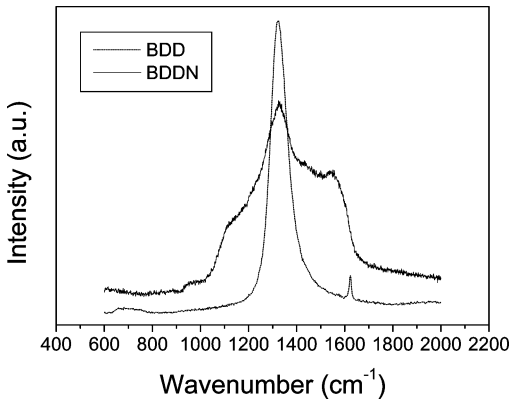

Figure 3. Raman spectra of the BDDN and BDD films (solid line, BDDN; dotted line, BDD).

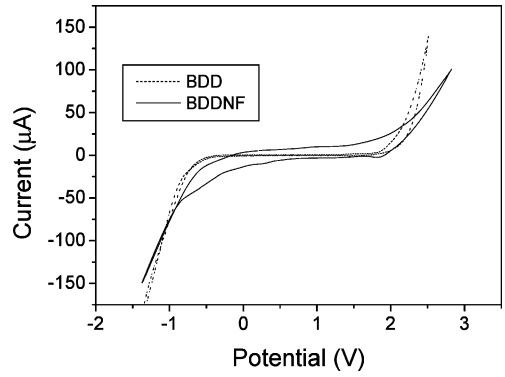

Figure 4. CVs of the BDDNF and BDD electrodes in 0.1 M H_2SO_4 solution with a scan rate of 100 mV s^{-1} (solid line, BDDNF; dotted line, BDD).

stretching modes of the sp^2-bonded carbon at the grain boundaries of nanocrystalline diamond.[28] The small quantity of sp^2 carbon may contribute to a good electric conductivity of the nanorods. A shoulder at 1130 cm^{-1} of the BDDN is often identified as a signature for high quality nanocrystalline diamond.[29]

Electrochemical Characterization. We took cyclic voltammetry measurements to characterize the BDDNF electrode. The planar BDD electrode was also used for comparison. As shown in Figure 4, the working potential window in 0.1 M H_2SO_4 remains wide for the BDDNF electrode in a way similar to the BDD electrode, while the BDDNF electrode presents higher double-layer capacitance than the BDD electrode; this feature is related to its nanostructure in essence that it results from the increased surface roughness factor.[30,31] Some further electrochemical characterizations with outer-sphere and inner-sphere redox couples ($Ru(NH_3)_6^{3+/2+}$ and $Fe(CN)_6^{3-/4-}$) were performed, and different voltammet-

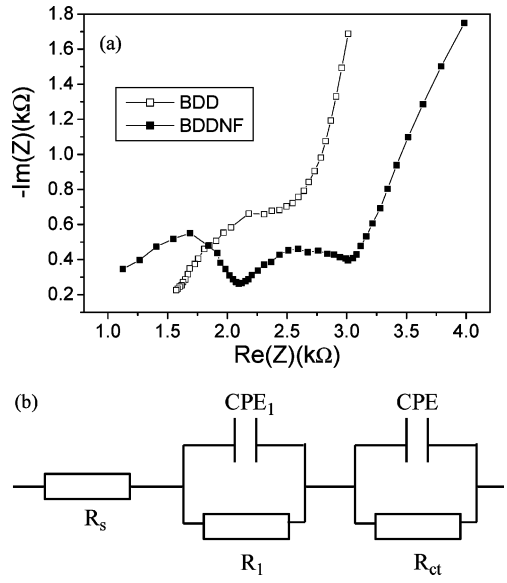

Figure 5. (a) Nyquist plots of the impedance for the BDDNF and BDD electrodes in 0.1 M H_2SO_4 (solid square, BDDNF; hollow square, BDD). (b) Equivalent circuit used for the BDDNF electrode.

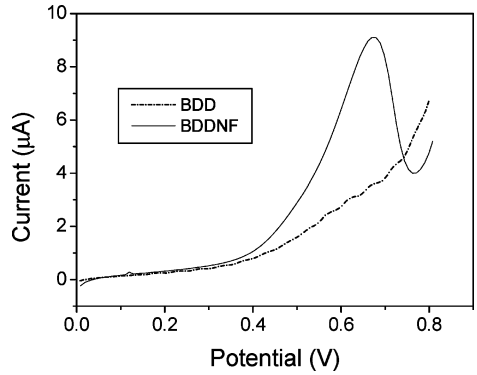

Figure 6. Positive potential scan in 0.1 M NaOH solution containing 0.1 mM glucose at the BDDNF and BDD electrodes with a scan rate of 50 mV s^{-1} (solid line, BDDNF; dotted line, BDD).

ric behavior on the BDDNF and BDD electrodes was observed (Supporting Information).

Furthermore, the impedance measurements of the BDDNF and BDD electrodes in 0.1 M H_2SO_4 were also investigated, and the Nyquist plots for both electrodes are shown in Figure 5a. As expected, marked differences are observed for the BDDNF and BDD electrodes in impedance characteristics. Compared to a semicircle and a linear region of the planar BDD electrode, the BDDNF electrode shows clearly two semicircles and a linear region, which are quite similar to the impedance behavior of porous electrodes.[32]

Taking the modeling of impedance of porous electrodes as references, we present the equivalent circuit of the BDDNF electrode in Figure 5b. For the BDDNF electrode, the double-layer capacitance is substituted by a constant phase element (CPE). We consider that the high frequency (HF) semicircle (CPE_1-R_1) is related to the porosity of the electrode and independent of the kinetics of the faradaic process, and the low frequency (LF) semicircle ($CPE-R_{ct}$) is related to the kinetics of the faradaic reaction.[33]

Amperometric Response to Glucose. Detection of glucose in 0.1 M NaOH aqueous solution at the BDDNF and BDD electrodes for comparison was first carried out with cyclic voltammetry measurements, and the results are shown in Figure 6. Almost no visual anodic peaks for glucose oxidation could be observed during the positive potential scan at the BDD electrode, whereas a well-defined current response for glucose is obtained at the BDDNF electrode at about 0.7 V (*vs* SCE) and the peak current is nearly 9 μA for 0.1 M of glu-

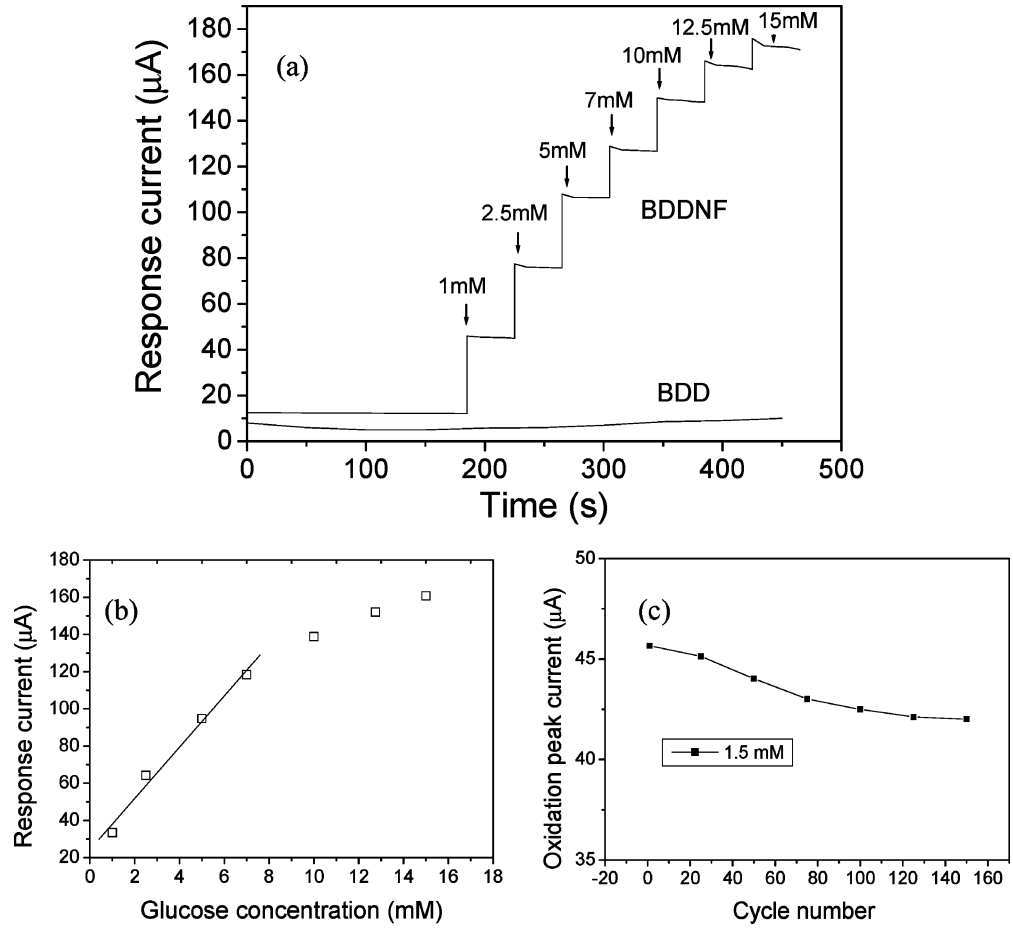

Figure 7. (a) Current−time responses of the BDDNF and BDD electrodes to a stirred solution containing 0.1 M NaOH at an applied potential of 0.7 V (*vs* SCE). (b) Calibration curve of the BDDNF electrode at a working potential of 0.7 V (*vs* SCE). (c) Long-term electrochemical cycling stability of the BDDNF electrode for 1.5 mM glucose.

cose. Such an improvement in glucose oxidation at the BDDNF electrode compared with the BDD electrode shows that the faradaic currents for glucose oxidation depend strongly on the surface structure of the electrodes. Obviously, the much enhanced oxidation current for glucose on the BDDNF electrode could be attributed to the influence of electrode roughness factors on one hand, and on the other hand, the enhanced oxidation current for glucose on the BDDNF electrode could be also due to the particular properties of the nanotexture; that is, the mass transport rate at the BDDNF electrode is expected to be enhanced significantly due to the increased electroactive electrode areas and the high current density at the rod-like-shaped electrode.[34]

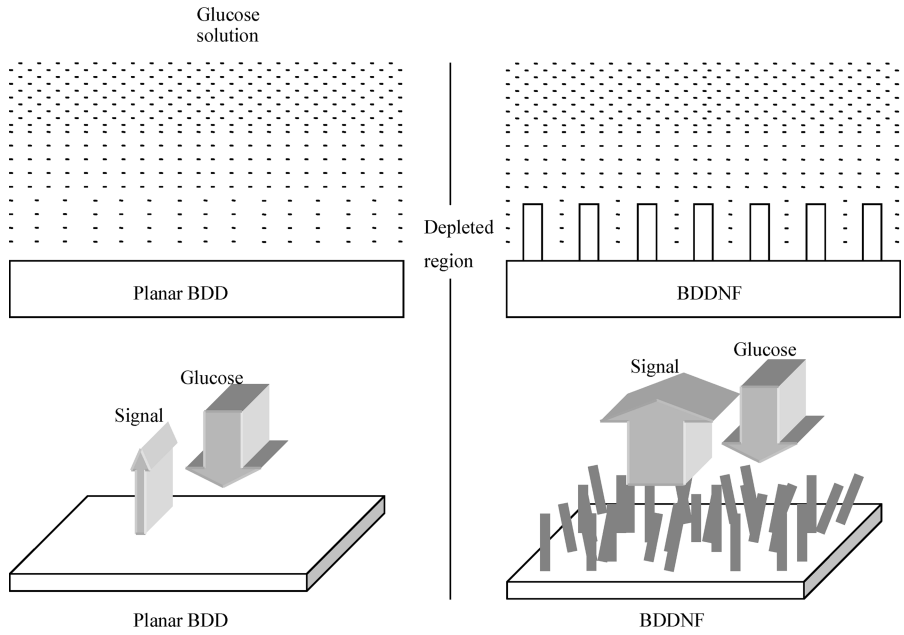

Figure 8. Schematic representation of glucose diffusion profiles at the planar BDD and BDDNF electrodes.

The amperometric responses at the BDDNF electrode at a working potential of 0.7 V (*vs* SCE) in 0.1 M NaOH solution for each successive addition of various concentrations of glucose are presented in Figure 7a. Glucose was added at the points indicated by arrows to the mentioned concentrations. Upon each addition of glucose, electrochemical responses were recorded while the solution was stirred constantly. As shown in Figure 7a, it is clear that the electrochemical response to glucose at the BDDNF electrode is very fast in reaching a dynamic equilibrium upon each addition of the sample solution, generating a steady-state current signal within a short time (less than 20 s). The calibration curve for the electrochemical responses of the BDDNF electrode to glucose at 0.7 V (*vs* SCE) in the concentration range between 0 and 15 mM is shown in Figure 7b. The response to glucose displays a linear range from 0 to 7 mM with a correlation coefficient (R) of 0.993 and a sensitivity of 8.1 μA mM^{-1} cm^{-2} (slope). The limit of detection was estimated at a signal-to-noise ratio of 3 to be 0.2 $\pm$ 0.01 μM.

The long-term stability of the BDDNF electrode in 1.5 mM glucose + 0.1 M NaOH solution was investigated (Figure 7c). Repetitive runs of the CV detection were realized by using the same procedure. The loss of the electrochemical activity was about 8% after 150 repetitive cycles, suggesting that the BDDNF electrode is relatively stable owing to its inertness of the H-terminated diamond surface. It is difficult for the substrates and analytes to adsorb on the electrode surface, which renders the electrode surface resistant to molecular adsorption (*i.e.*, deactivation and fouling). Therefore, the BDDNF electrode has good reproducibility and excellent stability.

The key idea for consideration of the electrochemical performance of the BDDNF electrode is based on the advantages that arise from its large surface area, high porosity, and highly conductive matrix. A schematic illustration of the effect of structure on electrochemical reaction of glucose is shown in Figure 8. It has been reported that the electro-oxidation for glucose is a kinetically controlled sluggish reaction.[23] The faradaic currents associated with a kinetic-controlled electrochemical reaction (for glucose) are sensitive to the nanoscopic surface area of the electrode, rather than its geometric area.[35,36] Therefore, according to this theory, the BDDNF electrode, with large surface area and mesoporous roughness due to its nanostructure, generates enlarged faradaic currents for glucose oxidation. Other possibilities which arise from nanocrystallite, sp^2 carbon sites have been eliminated (Supporting Information).

Selective Determination of Glucose in the Presence of AA and UA. The avoidance of endogenous interfering species is a big challenge in nonenzymatic glucose detection because a few of the structurally similar organic substances (for instance, AA and UA) are also simultaneously oxidized along with glucose at the electrode surface and, hence, give interfering electrochemical signals.[37] Figure 9a represents the CVs of the BDDNF electrode recorded in 1 mM glucose solution containing 1 mM of AA, which is one of the most serious interfering agents. A well-defined peak for glucose oxidation is successfully achieved without an overlap from that of AA oxidation, suggesting the feasibility of reliable

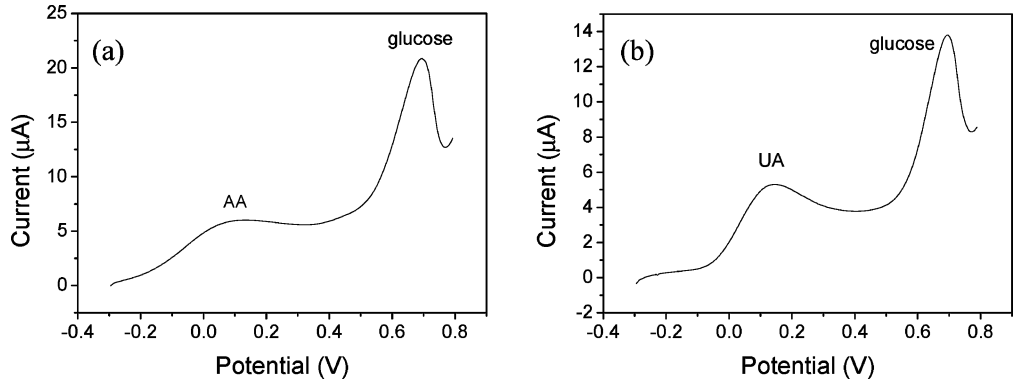

Figure 9. (a) Selectively voltammetric response to 1 mM glucose and 1 mM AA. (b) Selectively voltammetric response to 1 mM glucose and 0.2 mM UA at the BDDNF electrode in 0.1 M NaOH solution, with a scan rate of 50 mV s^{-1}.

determination of glucose free from AA interference. Similar measurements were also performed with 0.2 mM UA at the BDDNF electrode under the same experimental conditions (Figure 9b). It suggests that the BDDNF electrode is very favorable for the selective determination of glucose in the presence of AA and UA.

The electrochemical reactions for these interfering electroactive species (AA and UA) undergo a diffusion-controlled process. For a diffusion-controlled reaction, upon application of an anodic potential to the electrode, the surface concentration of the reactant will be immediately exhausted to zero; therefore, a concentration gradient of the reactants near the electrode surface is established. As a result, the faradaic currents of the reactants are proportional to the apparent geometric area of the electrode, regardless of the mesoporous roughness of the electrode.[38] This result also demonstrates that the selectivity and sensitivity of the BDDNF electrode for glucose detection can be further improved by using the BDDNF electrode with even higher roughness factors.

CONCLUSIONS

In conclusion, the BDDNF electrode was fabricated at a silicon wafer by EMD method and HFCVD technique. The BDDNF electrode was demonstrated as a nonenzymatic glucose biosensor by simply putting it into the glucose solution. Amperometric glucose sensing revealed that the BDDNF electrode with a three-dimensional structure exhibited high electrochemical activity to glucose oxidation in basic conditions. The linear range (up to 7 mM) and sensitivity of 8.1 μA mM^{-1} cm^{-2} of the BDDNF electrode to glucose oxidation and even the selectivity and stability were obviously good enough for the potential application in practical glucose detection. These promising results, combined with the biocompatibility of diamond, make this biosensor an exceptional choice for a wide range of biofunctionalization schemes and biomarker detection.

EXPERIMENTAL SECTION

Reagents. p-Type silicon wafers (100) were obtained from Shin-Etsu Chemical Co., Ltd. Glucose, AA, and UA were purchased from Aldrich. All chemicals were analytical grade and used without additional purification. Double distilled ultrapure water (>18 MΩ · cm) was used for all solution preparation. MBDD, NBDD, and GC were purchased from Element Six Co., Ltd.

Apparatus. The HFCVD system was purchased from Shanghai JiaoYou Diamond Coating Co., Ltd. The scanning electron microscopy was performed using a Hitachi Ultrahigh-Resolution S-4300 microscope. The transmission electron microscopy was taken with a JEM-200 (JEOL) microscope. The Raman spectroscopy was obtained using a Renishaw 1000 Raman spectrometer (Renishaw Ltd., UK).

BDDNF Preparation. The synthesis process of BDDNF is illustrated in Scheme 1. First, silicon nanowires were synthesized using EMD method according to ref 39. A p-type silicon wafer as a substrate was cleaned ultrasonically in acetone, ethanol, and pure water for 10 min. Then the cleaned silicon wafer was immersed in a mixture of 4.6 M HF and 0.02 M $AgNO_3$ aqueous solutions with equal volume. After etching for 40 min at 50 °C, the sample was dipped in 30 wt % HNO_3 aqueous solution for 60 s to remove the capped silver. Finally, the sample was rinsed with deionized water, dried in air, and used for further preparation.

The BDDNF electrode was prepared by depositing a boron-doped diamond thin film onto the as-fabricated SiNWs by HFCVD technology. The silicon wafer with as-grown SiNWs was used as the substrate. Before deposition, the substrate was pretreated ultrasonically in a suspension of diamond nanoparticles for 20 min. We used an acetone solution containing trimethyl borate (0.5% atoms ratio) as the carbon source. The carbon source/H_2 flow ratio was 200:50 sccm, and the growth duration was 60 min. The bias voltage was set at 4.5 V. The substrate was heated by tantalum wires with an ac power supply at a voltage of 20 V and the current of 75 A. The deposition power was kept at about 1500 W, and the pressure was maintained at 1 kPa. The diamond film that could be deposited on these SiNWs indicated that the as-etched SiNW surface contains abundant active sites and the adhesive diamond nanoparticles which reacted as diamond nuclei. Generally, diamond nucleation was formed very fast on these nuclei of the SiNWs, and growth was from these nuclei along the whole length of the SiNWs. A planar BDD film was also deposited under the same conditions for comparison.

Electrochemical Measurements. Electrochemical measurements were made using a 263 A potentiostat/galvanostat (Princeton, NJ) controlled by a PC. A three-electrode system consisting of a

working electrode (BDDNF, BDD), a saturated calomel electrode (SCE) reference electrode, and a Pt auxiliary electrode was connected to the workstation. All measurements were taken at room temperature. Impedance spectroscopy measurements were carried out with a FRD 100 frequency response detector (Princeton, NJ) connected to the same potentiostat/galvanostat. A normal planar BDD electrode prepared under the same conditions from HFCVD always works for comparison. Before use, the working electrodes (BDDNF, BDD) were washed under ultrasonication in 2-propanol followed by ultrapure water for 10 min, respectively. Each cyclic voltammetry was performed in a solution of 10 mL volume. The electrode geometric surface area exposed to the solution was 0.1 cm^2.

Before electrochemical detection of glucose, the electrodes were cycled 10 times in 0.1 M NaOH between 0 and 1.5 V (*vs* SCE) until a reproducible background voltammogram was obtained. Amperometric measurements of glucose were carried out in a 0.1 M NaOH solution at a desired potential (0.7 V *vs* SCE). The response currents at each glucose concentration were recorded after a steady state was reached.

Acknowledgment. We gratefully acknowledge the Major Research Development Program of China (No. 2006CB933000), and National Natural Science Foundation of China (207731500).

Supporting Information Available: Detailed information includes the experimental results of (1) comparison of CVs in $Ru(NH_3)_6^{3+/2+}$ and $Fe(CN)_6^{3-/4-}$ at the BDDNF and planar BDD electrodes (Figure S1), (2) CVs of glucose on typical MBDD and NBDD electrodes (Figure S2), and (3) CVs of glucose on a GC electrode, and a BDD (with more sp^2 carbon) electrode (Figure S3). Relevant discussions are also included. This material is available free of charge *via* the Internet at http://pubs.acs.org.

REFERENCES AND NOTES

1. Pleskov, Y. V.; Sakharova, A. Y.; Krotova, M. D. Photoelectrochemical Properties of Semiconductor Diamond. *J. Electroanal. Chem.* **1987**, *228*, 19–27.
2. Kapałka, A.; Fóti, G.; Comniellis, C. The Importance of Electrode Material in Environmental Electrochemistry Formation and Reactivity of Free Hydroxyl Radicals on Boron-Doped Diamond Electrodes. *Electrochim. Acta* **2009**, *54*, 2018–2023.
3. Poh, W. C.; Loh, K. P. Biosensing Properties of Diamond and Carbon Nanotubes. *Langmuir* **2004**, *20*, 5484–5492.
4. Zhou, Y. L.; Tian, R. H.; Zhi, J. F. Amperometric Biosensor Based on Tyrosinase Immobilized on a Boron-Doped Diamond Electrode. *Biosens. Bioelectron.* **2007**, *22*, 822–828.
5. Hian, L. C.; Grehan, K. J.; Compton, R. G.; Foord, J. S.; Marken, F. Influence of Thin Film Properties on the Electrochemical Performance of Diamond Electrodes. *Diamond Relat. Mater.* **2003**, *12*, 590–595.
6. Wu, L. N.; Zhang, X. J.; Ju, H. X. Detection of NADH and Ethanol Based on Catalytic Activity of Soluble Carbon Nanofiber with Low Overpotential. *Anal. Chem.* **2007**, *79*, 453–458.
7. Arumugam, P. U.; Chen, H.; Cassell, A. M.; Li, J. Dielectrophoretic Trapping of Single Bacteria at Carbon Nanofiber Nanoelectrode Arrays. *J. Phys. Chem. A* **2007**, *111*, 12772–12777.
8. Zheng, H. J.; Ma, C. A.; Wang, W.; Huang, J. G. Nanorod Tungsten Carbide Thin Film and Its Electrocatalytic Activity for Nitromethane Electroreduction. *Electrochem. Commun.* **2006**, *8*, 977–981.
9. Lee, H. J.; Yoon, S. W.; Kim, E. J.; Park, J. H. *In-Situ* Growth of Copper Sulfide Nanocrystals on Multiwalled Carbon Nanotubes and Their Application as Novel Solar Cell and Amperometric Glucose Sensor Materials. *Nano Lett.* **2007**, *7*, 778–784.
10. Vamvakaki, V.; Tsagaraki, K.; Chaniotakis, N. Carbon Nanofiber-Based Glucose Biosensor. *Anal. Chem.* **2006**, *78*, 5538–5542.
11. Baker, S. E.; Colavita, P. E.; Tse, K.-Y.; Hamers, R. J. Functionalized Vertically Aligned Carbon Nanofibers as Scaffolds for Immobilization and Electrochemical Detection of Redox-Active Proteins. *Chem. Mater.* **2006**, *18*, 4415–4422.
12. Baik, E.-S.; Baik, Y.-J.; Lee, S. W.; Jeon, D. Fabrication of Diamond Nano-whiskers. *Thin Solid Films* **2000**, *377*, 295–298.
13. Baik, E.-S.; Baik, Y.-J.; Jeon, D. Aligned Diamond Nanowhiskers. *J. Mater. Res.* **2000**, *15*, 923–926.
14. Yang, N. J.; Uetsuka, H.; Osawa, E.; Nebel, C. E. Vertically Aligned Nanowires from Boron-Doped Diamond. *Nano Lett.* **2008**, *8*, 3572–3576.
15. Okuyama, S.; Matsushita, S. I.; Fujishima, A. Periodic Submicrocylinder Diamond Surfaces Using Two-Dimensional Fine Particle Arrays. *Langmuir* **2008**, *18*, 8282–8287.
16. Masuda, H.; Yanagishita, T.; Yasui, K.; Nishio, K.; Yagi, I.; Rao, T. N.; Fujishima, A. Synthesis of Well-Aligned Diamond Nanocylinders. *Adv. Mater.* **2001**, *13*, 247–249.
17. Barnard, A. S.; Terranova, M. L.; Rossi, M. Density Functional Study of H-Induced Defects as Nucleation Sites in Hybrid Carbon Nanomaterials. *Chem. Mater.* **2005**, *17*, 527–535.
18. Zhao, Y.; Fan, L. Z.; Zhong, H. Z.; Li, Y. F.; Yang, S. H. Platinum Nanoparticle Clusters Immobilized on Multiwalled Carbon Nanotubes: Electrodeposition and Enhanced Electrocatalytic Activity for Methanol Oxidation. *Adv. Funct. Mater.* **2007**, *17*, 1537–1541.
19. Nair, S.; Kim, J.; Crawford, B.; Kim, S. H. Improving Biocatalytic Activity of Enzyme-Loaded Nanofibers by Dispersing Entangled Nanofiber Structure. *Biomacromolecules* **2007**, *8*, 1266–1270.
20. Suffredini, H. B.; Tricol, V.; Avaca, L. A.; Vatistas, N. Sol−Gel Method to Prepare Active Pt-RuO_2 Coatings on Carbon Powder for Methanol Oxidation. *Electrochem. Commun.* **2004**, *6*, 1025–1028.
21. Doménech, A.; Alarcón, J. Microheterogeneous Electrocatalytic Chiral Recognition at Monoclinic Vanadium-Doped Zirconias: Enantioselective Detection of Glucose. *Anal. Chem.* **2007**, *79*, 6742–6751.
22. Lu, J.; Do, I.; Drzal, L. T.; Worden, R. M.; Lee, I. Nanometal-Decorated Exfoliated Graphite Nanoplatelet Based Glucose Biosensors with High Sensitivity and Fast Response. *ACS Nano* **2008**, *2*, 1825–1832.
23. Park, S. J.; Chung, T. D.; Kim, H. C. Nonenzymatic Glucose Detection Using Mesoporous Platinum. *Anal. Chem.* **2003**, *75*, 3046–3049.
24. Yuan, J. H.; Wang, K.; Xia, X. H. Highly Ordered Platinum-Nanotube Arrays for Amperometric Glucose Sensing. *Adv. Funct. Mater.* **2005**, *15*, 803–809.
25. Wang, L.; Zhu, X. D. Effect of Substrate Facets on Homoepitaxial Growth of Diamonds during Plasma-Assisted Hot Filament Chemical Vapor Deposition. *Diamond Relat. Mater.* **2007**, *16*, 637–641.
26. Schade, A.; Rosiwal, S. M.; Singer, R. F. Influence of Surface Topography of HF-CVD Diamond Films on Self-Mated Planar Sliding Contacts in Dry Environments. *Surf. Coat. Technol.* **2007**, *201*, 6197–6205.
27. Tachibana, T.; Yokota, Y.; Miyata, K.; Onishi, K.; Kobashi, K.; Tarutani, M.; Takai, Y.; Shimizu, R.; Shintani, Y. Diamond Films Heteroepitaxially Grown on Platinum(111). *Phys. Rev. B* **1997**, *56*, 15967–15981.
28. Ferrari, A. C.; Robertson, J. Interpretation of Raman Spectra of Disordered and Amorphous Carbon. *Phys. Rev. B* **2000**, *61*, 14095–14107.
29. Ferrari, A. C.; Robertson, J. Origin of 1150-cm^{-1} Raman Mode in Nanocrystalline Diamond. *Phys. Rev. B* **2001**, *63*, 121405-1–121405-4.
30. Cachet, C.; Wiart, R. Couple Axial Gradients of Potential and Concentration in a Cylindrical Pore Electrode: An Impedance Model. *J. Electroanal. Chem.* **1985**, *195*, 21–37.
31. Susanti, D.; Tsai, D.-S.; Huang, Y.-S.; Korotcov, A.; Chung, W.-H. Structures and Electrochemical Capacitive Properties of RuO_2 Vertical Nanorods Encased in Hydrous RuO_2. *J. Phys. Chem. C* **2007**, *111*, 9530–9537.

32. Lasia, A. Impedance of Porous Electrodes. *J. Electroanal. Chem.* **1995**, *397*, 27–33.
33. Hitz, C.; Lasia, A. Experimental Study and Modeling of Impedance of the Her on Porous Ni Electrodes. *J. Electroanal. Chem.* **2001**, *500*, 213–222.
34. Gollas, B.; Elliot, J. M.; Bartlett, P. N. Electrodeposition and Properties of Nanostructured Platinum Films Studied by Quartz Crystal Impedance Measurements at 10 MHz. *Electrochim. Acta* **2000**, *45*, 3711–3724.
35. Watanabe, T.; Ivandini, T. A.; Makide, Y.; Fujishima, A.; Einaga, Y. Selective Detection Method Derived from a Controlled Diffusion Process at Metal-Modified Diamond Electrodes. *Anal. Chem.* **2006**, *78*, 7857–7860.
36. Bai, Y.; Sun, Y. Y.; Sun, C. Q. Pt−Pb Nanowire Array Electrode for Enzyme-Free Glucose Detection. *Biosens. Bioelectron.* **2008**, *24*, 579–585.
37. Lee, J. W.; Park, S.-M. Direct Electrochemical Assay of Glucose Using Boron-Doped Diamond Electrodes. *Anal. Chim. Acta* **2005**, *545*, 27–32.
38. Bard, A. J.; Faulkner, L. R. *Electrochemical Methods: Fundamentals and Applications*; Wiley: New York, 2001.
39. Peng, K. Q.; Yan, Y. J.; Gao, S. P.; Zhu, J. Synthesis of Large-Area Silicon Nanowire Arrays *via* Self-Assembling Nanoelectrochemistry. *Adv. Mater.* **2002**, *14*, 1164–1167.